A numerical study of nanofluid natural convection in a cubic enclosure with a circular and an ellipsoidal cylinder

J. Ravnik *, L. Škerget

Faculty of Mechanical Engineering, University of Maribor, Smetanova 17, SI-2000 Maribor, Slovenia

ABSTRACT

In this paper we develop a numerical method and present results of simulations of flow and heat transfer of nanofluids. We consider a heated circular and elliptical cylinder in a cooled cubic enclosure. Natural convection, which drives the flow, and heat transfer are simulated for different temperature differences and enclosure inclination angles. Steady laminar regime is considered with Rayleigh number values up to a million. Al_2O_3, Cu and TiO_2 nanofluids are considered, as well as pure water and air for validation purposes. Properties of nanofluids are considered to be constant throughout the domain and are estimated for different nanoparticle volume fractions (0.1 and 0.2).

In order to simulate nanofluids, an in-house numerical method was developed based on the solution of 3D velocity–vorticity formulation of Navier–Stokes equations. The boundary element method is used to solve the governing equations. In the paper, special consideration is given to the estimation of the boundary value of vorticity on an arbitrary curved surface.

The results show highest heat transfer enhancement in the conduction dominated flow regime, where the enhanced thermal properties of nanofluids play an important role. When convection is the dominant heat transfer mechanism, the using nanofluids yields a smaller increase in heat transfer efficiency. Comparison of 2D and 3D results reveals consistently lower heat transfer rates in the 3D case. As the enclosure is tilted against gravity, the flow symmetry around an elliptical cylinder is lost and the overall heat transfer increases.

© 2015 Elsevier Ltd. All rights reserved.

1. Introduction

Cooling is one of the major challenges in development of efficient devices. Natural convection is used to design many devices, for example, heat exchangers and electronics coolers. Study of natural convection in such devices was started by De Vahl Davies [6], who proposed the now classical problem of a differentially heated cavity. He considered an enclosure, where one wall is heated to a constant temperature and a wall on the opposite side is cooled to a constant temperature. Due to the temperature difference, natural convection develops in the enclosure. Many engineering applications are geometrically more complicated and thus more recently, attention has shifted to enclosures with hot bodies embedded within [9]. Depending on the temperature difference, the natural convection that develops, may be steady and laminar for low temperature differences, while for higher temperature differences transition to turbulence may be observed.

Choice of a working fluid is very important, as its thermal properties determine heat transfer characteristics. As thermal conductivity of water, oil and other working fluids are low, Choi [4] introduced nanofluids. Nanofluid is a suspension consisting of uniformly dispersed and suspended nanometre-sized (10–50 nm) particles in base fluid. Nanofluids have a very high thermal conductivity at a very low nanoparticle concentrations and exhibit considerable enhancement of convection [35]. A wide variety of experimental and theoretical investigations have been performed, as well as several nanofluid preparation techniques have been proposed [32].

Research in the use of nanofluids for natural convection type application has been intensified in recent years [31,18,27]. Hu et al. [11] considered a square enclosure filled with nanofluid and compared experiments and numerical simulations for different nanoparticle concentrations. Oztop and Abu-Nada [21] performed a 2D study of natural convection of various nanofluids in partially heated rectangular cavities, reporting that the type of nanofluid is a key factor for heat transfer enhancement. They obtained best results with Cu nanoparticles. The same researchers [2] examined the effects of inclination angle on natural convection

---

* Corresponding author.
E-mail addresses: jure.ravnik@um.si (J. Ravnik), leopold.skerget@um.si (L. Škerget).

in enclosures filled with Cu–water nanofluid. They reported that the effect of nanofluid on heat enhancement is more pronounced at low Rayleigh numbers. Hwang et al. [12] studied natural convection of a water based Al_2O_3 nanofluid in a rectangular cavity heated from below. They investigated convective instability of the flow and heat transfer and reported that the natural convection of a nanofluid becomes more stable when the volume fraction of nanoparticles increases. Ho et al. [10] studied effects on nanofluid heat transfer due to uncertainties of viscosity and thermal conductivity in a buoyant enclosure. They demonstrated that usage of different models for estimation of viscosity and thermal conductivity does indeed have a significant impact on heat transfer. Natural convection of nanofluids in an inclined differentially heated square enclosure was studied by Ögüt [20], using polynomial differential quadrature method. Kim et al. [15] studied $2D$ natural convection of air around a circular cylinder within a square enclosure. Sheremet et al. [28] considered natural convection in a $3D$ porous enclosure filled with a nanofluid and compared homogeneous nanoparticle distribution model with a inhomogeneous model. Most of the studies in the literature were done in 2D. In this paper we present development of a $3D$ nanofluid flow simulation algorithm.

Several numerical methods have been proposed for the simulation of nanofluids. Garoosi [8] carried out a numerical study of natural and mixed convection heat transfer of nanofluid in a two-dimensional square cavity with several pairs of heat source-sinks using the finite volume method. Control volume based finite element method was used by Seyyedi et al. [26] to simulate the natural convection heat transfer of Cu–water nanofluid in an annulus enclosure. El Abdallaoui et al. [1] used the lattice Boltzmann method for numerical simulation of natural convection between a decentered triangular heating cylinder and a square outer cylinder filled with a pure fluid or a nanofluid. Elshehabey et al. [7] developed a finite difference method for natural convection in an inclined L-shaped enclosure filled with Cu–water nanofluid that operates under differentially heated walls in the presence of an inclined magnetic field. Kefayati [13] used a finite difference lattice Boltzmann method heat transfer and entropy generation due to laminar natural convection in a square cavity.

In this paper we present a boundary element method based algorithm for simulation of flow and heat transfer of nanofluids. We formulate the Navier–Stokes equations in velocity–vorticity form and couple them with the energy conservation equation. Daube [5] pointed out that the correct evaluation of boundary vorticity values is essential for conservation of mass when using the velocity vorticity formulation. Several different methods were considered for estimation of the vorticity on the boundary. Wong and Baker [33] used a second-order Taylor series to determine the boundary vorticity values explicitly. Daube [5] used an influence matrix technique to enforce both the continuity equation and the definition of the vorticity in the treatment of the $2D$ incompressible Navier–Stokes equations. Liu [16] recognised that the problem is even more severe when he extended it to three dimensions. Lo et al. [17] used the differential quadrature method. Škerget et al. [30] proposed the usage of single domain BEM to obtain a solution of the kinematics equation in tangential form for the unknown boundary vorticity values and used it in 2D. This work was extended into $3D$ using a linear interpolation by Žunič et al. and Ravnik et al. [25] for simple geometries. In this paper we extend these methods for determination of boundary vorticity at an arbitrarily shaped surface.

2. Problem description

A heated cylinder is inserted into an enclosure with four cooled walls. Front and back walls are perfectly insulated (adiabatic). All walls have a no-slip boundary condition applied for velocity. The heat is transferred from the cylinder to the fluid causing density changes that result in buoyancy forces. Natural convection develops – the fluid rises around the cylinder and transports heat towards the cold walls. The heat flux depends on the type of fluid (air, water and nanofluids in this work), the shape of the cylinder and the orientation of the enclosure with respect to gravity.

The centre of the cylinder is located at the centre of the enclosure. The shape of the base of the cylinder is an ellipse with major semi-axis a and minor semi axis b. They are defined as

$$a = 0.2L, \quad b = a\sqrt{1 - e^2}, \tag{1}$$

where e is the eccentricity of the ellipse and the length of the cylinder is L. The enclosure is cubic with a volume of L^3. It is tilted with respect to gravity with an angle of γ. The temperature of the cylinder is constant T_h and the temperature of the cold walls is also constant, T_c (see Fig. 1).

3. Governing equations

We consider water based nanofluids, as well as pure water and air for validation and comparisons. Thermophysical properties of solid nanoparticles and all fluids are given in Table 1. Water and nanoparticles are in thermal equilibrium and no slip occurs between them. We assume the nanofluid to be incompressible. Natural convection exhibited by the nanofluids in our simulations is laminar and steady. Effective properties of the nanofluid are: density ρ_{nf}, dynamic viscosity μ_{nf}, heat capacitance $(c_p)_{nf}$, thermal expansion coefficient β_{nf} and thermal conductivity k_{nf}, where subscript nf is used to denote effective i.e. nanofluid properties. The properties are all assumed constant throughout the flow domain. Pure fluid properties will be denoted by the subscript f.

Dimensionless velocity $\vec{v}$, location vector $\vec{r}$, vorticity $\vec{\omega}$, temperature T and gravity $\vec{g}$ were employed by introducing

$$\vec{v} \rightarrow \frac{\vec{v}^\star}{v_0}, \quad \vec{r} \rightarrow \frac{\vec{r}^\star}{L}, \quad \vec{\omega} \rightarrow \frac{\vec{\omega}^\star L}{v_0}, \quad T \rightarrow \frac{T^\star - T_c}{T_h - T_c}, \quad \vec{g} \rightarrow \frac{\vec{g}^\star}{g_0}, \tag{2}$$

where, $v_0 = \frac{k_f}{(\rho c_p)_f L}$ is the characteristic velocity and $g_0 = 9.81$ m/s^2.

The nondimensional steady velocity–vorticity formulation of Navier–Stokes equations for simulation of nanofluids consists of
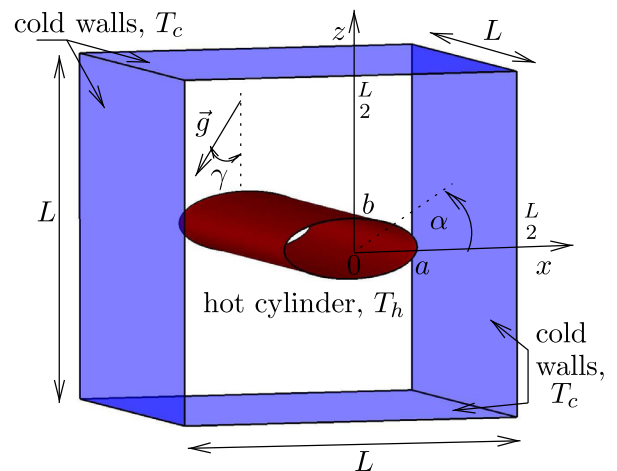

Fig. 1. Computational domain and coordinate system with boundary conditions. The angle α measures a location around the circumference of the cylinder. The angle γ measures the tilt of the enclosure with respect to the gravity vector. The front and back walls ($y = 0$ and $y = L$) are adiabatic.

Table 1
Thermophysical properties of pure fluids, solid nanoparticles and water based nanofluids. Effective nanofluid properties have been estimated using models in Eqs. (7)–(11).

	c_p [J/kg K]	ρ [kg/m³]	k [W/m K]	β [$\cdot 10^{-5}$ K⁻¹]	μ [mm²/s]
Pure fluids					
Air	1005	1.205	0.0257	3.43	15.11
Water	4179	997.1	0.613	21	0.912
Solid nanoparticles [21]					
Cu	385	8933	400	1.67	
Al₂O₃	765	3970	40	0.85	
TiO₂	686.2	4250	8.9538	0.9	
Water based nanofluids, $\varphi = 0.1$, Eqs. (7)–(11)					
Cu	2286	1791	0.816	11.36	1.187
Al₂O₃	3132	1294	0.807	14.82	1.187
TiO₂	3056	1322	0.777	14.54	1.187
Water based nanofluids, $\varphi = 0.2$, Eqs. (7)–(11)					
Cu	1556	2584	1.070	7.636	1.593
Al₂O₃	2476	1592	1.047	10.95	1.593
TiO₂	2377	1648	0.973	10.63	1.593

the kinematics equation, the vorticity transport equation and the energy equation [23]:

$$\nabla^2 \vec{v} + \vec{\nabla} \times \vec{\omega} = 0, \tag{3}$$

$$(\vec{v} \cdot \vec{\nabla})\vec{\omega} = (\vec{\omega} \cdot \vec{\nabla})\vec{v} + Pr \frac{\mu_{nf}}{\mu_f} \frac{\rho_f}{\rho_{nf}} \nabla^2 \vec{\omega} - PrRa \frac{\beta_{nf}}{\beta_f} \vec{\nabla} \times T\vec{g}, \tag{4}$$

$$(\vec{v} \cdot \vec{\nabla})T = \frac{k_{nf}}{k_f} \frac{(\rho c_p)_f}{(\rho c_p)_{nf}} \nabla^2 T. \tag{5}$$

The flow and heat transfer of a nanofluid is thus defined by specifying the pure fluid Rayleigh and Prandtl number values. They are defined as

$$Ra = \frac{g_0 \beta_f \Delta T L^3 \rho_f (\rho c_p)_f}{\mu_f k_f}, \quad Pr = \frac{\mu_f c_p}{k_f}. \tag{6}$$

The nanofluid properties are evaluated using the following models. Density of the nanofluid is calculated using particle volume fraction φ and densities of pure fluid ρ_f and of solid nanoparticles ρ_s as:

$$\rho_{nf} = (1 - \varphi)\rho_f + \varphi \rho_s. \tag{7}$$

The effective dynamic viscosity of a fluid of dynamic viscosity μ_f containing a dilute suspension of small rigid spherical particles, is given by Brinkman [3] as

$$\mu_{nf} = \frac{\mu_f}{(1 - \varphi)^{2.5}}. \tag{8}$$

The heat capacitance of the nanofluid can be expressed as [14]:

$$(\rho c_p)_{nf} = (1 - \varphi)(\rho c_p)_f + \varphi(\rho c_p)_s. \tag{9}$$

Similarly, the nanofluid thermal expansion coefficient can be written as $(\rho \beta)_{nf} = (1 - \varphi)(\rho \beta)_f + \varphi(\rho \beta)_s$, which may be, by taking into account the definition of ρ_{nf}, written as:

$$\beta_{nf} = \beta_f \left[\frac{1}{1 + \frac{(1-\varphi)\rho_f}{\varphi \rho_s} \frac{\beta_s}{\beta_f}} + \frac{1}{1 + \frac{\varphi}{1-\varphi} \frac{\rho_s}{\rho_f}} \right]. \tag{10}$$

The effective thermal conductivity of the nanofluid is approximated by the Maxwell–Garnett formula [19]

$$k_{nf} = k_f \frac{k_s + 2k_f - 2\varphi(k_f - k_s)}{k_s + 2k_f + \varphi(k_f - k_s)}. \tag{11}$$

This formula is valid only for spherical particles, since it does not take into account the shape of particles. Thus, our macroscopic modelling of nanofluids is restricted to spherical nanoparticles and it is suitable for small temperature gradients [29].

4. Numerical procedure

The governing equations were solved for heat and fluid flow by an in-house boundary element based algorithm [24,23,36,22]. The algorithm solves the velocity–vorticity formulation of Navier–Stokes equations. It requires known velocity and temperature boundary conditions. The problem considered in this paper has known Dirichlet boundary conditions for velocity (no-slip at the walls) and Dirichlet (temperature on the cylinder and walls) and Neumann (zero heat flux on two walls) boundary conditions for temperature. Boundary conditions for vorticity are unknown.

In the first step, the algorithm estimates boundary vorticity values using single domain BEM on the kinematics equation (3). This step is described in detail in Section 4.1. Secondly, using sub-domain BEM solution of the kinematics equation (3) the velocity in the domain is calculated. Thirdly, the energy equation (5) is solved for domain temperature values using sub-domain BEM. Lastly, the vorticity transport equation (4) is solved for domain vorticity values using sub-domain BEM. The procedure is repeated until convergence for all field functions is achieved. Convergence criterion of 10^{-5} was used. It is calculated as the RMS difference between field functions in two subsequent iterations. Under-relaxation is used. A value of 0.1 is used for problems with low Rayleigh number value and 0.01 for problems with high Rayleigh number value.

4.1. Vorticity boundary conditions for an arbitrary 3D surface

Several different approaches have been proposed for the determination of vorticity on the boundary. We propose the usage of singular integral kinematics equation. In this work, we extend the approach for determining boundary vorticity on an arbitrary 3D surface.

The normal component of vorticity at the boundary is usually known. If we consider a wall, then the velocity at the wall is either zero or we know the value of slip velocity. Thus, the normal component of vorticity may be calculated directly from the known velocity distribution at the wall. This is possible due to the fact that in order to calculate the normal component of vorticity only tangential components of the velocity are needed. The same reasoning applies at the inlets and outlets as well, since the velocity profile is known there. In the case of symmetry or free slip boundary conditions, the flux of normal component of vorticity is zero. This can be used in the vorticity transport equation and as a results, the normal component of boundary vorticity can be calculated there.

For an arbitrary surface, such as the cylinder in our case, the normal component of vorticity is calculated using Cartesian vorticity components and the unit normal to the surface, i.e. $\omega_n = \vec{n} \cdot \vec{\omega} = \sum_i n_i \omega_i$, where $i = x, y, z$. Since we know that $\omega_n = 0$ at the no-slip surface and $\vec{n}$ changes along the surface, we propose the following strategy to find ω_x, ω_y and ω_z.

The singular boundary integral representation for the velocity vector can be formulated by using the Green theorems for scalar functions, or weighting residuals technique. Following Wu and Thompson [34], Škerget et al. [30] derived the following integral form of the kinematics equation, employing the derivatives of the fundamental solution:

$$c(\vec{\xi})\vec{v}(\vec{\xi}) + \int_\Gamma \vec{v}(\vec{n} \cdot \vec{\nabla}u^\star)d\Gamma = \int_\Gamma \vec{v} \times (\vec{n} \times \vec{\nabla}u^\star)d\Gamma + \int_\Omega (\vec{\omega} \times \vec{\nabla}u^\star)d\Omega, \tag{12}$$

where $u^\star = u^\star(\vec{\xi}, \vec{r})$ is the elliptic Laplace fundamental solution, $\vec{\xi}$ is the source point on boundary Γ, $\vec{r}$ integration point in domain Ω (including Γ), $c(\vec{\xi})$ geometry coefficient and $\vec{n}$ outward pointing normal to the boundary. Geometry coefficient can be generally

computed as $\Theta/4\pi$, where Θ is the internal solid angle at point $\vec{\xi}$ in steradians. The Laplace fundamental solution is $u^{\star}(\vec{\xi}, \vec{r}) = 1/4\pi|\vec{\xi} - \vec{r}|$.

To obtain discrete form of integral equation we divide computational domain Ω into domain elements and its boundary Γ into boundary elements. Domain elements used are hexahedra with 27 nodes enabling quadratic interpolation. Boundary elements used are sides of domain hexahedra with 9 nodes. They also enable quadratic interpolation. A function, e.g. temperature, is interpolated over a boundary elements as $T = \sum \Xi_i T_i$, inside each domain element as $T = \sum \Phi_i T_i$. Functions Ξ_i and Φ_i are interpolation functions.

After a choice of the source point $\vec{\xi}$ in (12) has been made and interpolation of functions used, the integrals in (12) depend only on the geometry and the fundamental solution. They may be calculated and stored in matrices. The boundary integrals on the left hand side are stored in the $[H]$ matrix, the boundary integrals on the right hand side in the $[\vec{H}^t]$ matrix and the domain integrals on the right hand side are stored in the $[\vec{D}]$ matrices. For each source point a row in the matrices is calculated:

$$[H] = \int_{\Gamma} \Xi_i (\vec{n} \cdot \vec{\nabla} u^{\star}) d\Gamma, \quad [\vec{H}^t] = \int_{\Gamma} \Xi_i (\vec{n} \times \vec{\nabla} u^{\star}) d\Gamma, \tag{13}$$

$$[\vec{D}] = \int_{\Omega} \Phi_i \vec{\nabla} u^{\star} d\Omega. \tag{14}$$

The $[H]$ matrix holds integrals of normal derivatives of the fundamental solution, $[\vec{H}^t]$ tangential derivatives and $[\vec{D}]$ the gradient of the fundamental solution. Thus the discrete version of Eq. (12) may be written as

$$[H]\{\vec{v}\} = \{\vec{v}\} \times [\vec{H}^t] + \{\vec{\omega}\} \times [\vec{D}], \tag{15}$$

where curly brackets denote vectors of nodal values of field functions. In order to obtain a system of linear equations, the source point is placed into all boundary nodes. Thus the number of rows in all matrices is equal to the number of boundary nodes. The number of columns in $[H]$ and $[\vec{H}^t]$ is also equal to the number of boundary nodes since they are multiplied by boundary velocity values. On the other hand, the number of columns in $[\vec{D}]$ is equal to the number of all nodes, as $[\vec{D}]$ is multiplied by vorticity in the domain and on the boundary.

In order to use Eq. (15) to solve for boundary vorticity values we decompose the vorticity vector into two parts in the following way $\{\omega_i\} = \{\omega_i\}_{\Gamma} + \{\omega_i\}_{\Omega'}$. In the vector $\{\omega_i\}_{\Gamma}$ only the boundary vorticity values are non-zero and in the vector $\{\omega_i\}_{\Omega'}$ only the domain vorticity values are non-zero. The subscript Γ stands for boundary nodes only and Ω' stands for interior nodes only (without boundary nodes). Furthermore, one must set up the system in such a way, that the system matrix is non-singular. Since we are dealing with boundary element method, the system matrix may contain a normal derivative of the fundamental solution for the integral kernel. The integral kernel in the matrices $[D_x], [D_y], [D_z]$ are the components of the gradient of the fundamental solution. The normal derivative may be written as $[n_x][D_x] + [n_y][D_y] + [n_z][D_z] = [\vec{n}] \cdot [\vec{D}]$, where $[n_x], [n_y]$ and $[n_z]$ are diagonal matrices of unit normal vector components $\vec{n} = (n_x, n_y, n_z)$ for each boundary source point.

To obtain such a system, we perform a vector product of (15) by normal vector $[\vec{n}]$

$$[H]([\vec{n}] \times \{\vec{v}\}) = [\vec{n}] \times \left(\{\vec{v}\} \times [\vec{H}^t] + \{\vec{\omega}\} \times [\vec{D}]\right) \tag{16}$$

and after using $[\vec{n}] \times (\{\vec{\omega}\} \times [\vec{D}]) = ([\vec{n}] \cdot [\vec{D}])\{\vec{\omega}\} - [\vec{D}]\{\omega_n\}$ and $\{\vec{\omega}\} = \{\vec{\omega}\}_{\Gamma} + \{\vec{\omega}\}_{\Omega'}$ and rearranging we obtain

$$\left([\vec{n}] \cdot [\vec{D}]\right)\{\vec{\omega}\}_{\Gamma} = [\vec{D}]\{\omega_n\} - \left([\vec{n}] \cdot [\vec{D}]\right)\{\vec{\omega}\}_{\Omega'} - \left([\vec{n}] \cdot [\vec{H}^t]\right)\{\vec{v}\}$$
$$+ [\vec{H}^t]\{v_n\} + [H]([\vec{n}] \times \{\vec{v}\}). \tag{17}$$

In Eq. (17), all three equations for individual components of boundary vorticity are non-singular. However, they can only be used to solve for tangential components of the boundary vorticity, since the equation for normal component of boundary vorticity is identically equal to zero. This can be seen, if we consider a boundary located in plane $y - z$ with the unit normal $\vec{n} = \{1, 0, 0\}$. In this case ω_x is the normal component of the vorticity and v_x is the normal component of velocity. We observe that all terms in Eq. (17) for ω_x are either zero or cancel each other. Thus, the equation is identically equal to zero and it can not be used for the solution of the normal component of vorticity.

Finally, the algorithm for determining the boundary vorticity is as follows. At each source point, which is located at the boundary, compare $|n_x|, |n_y|$ and $|n_z|$ to find the largest component of the normal vector. Use Eq. (17) to find the other two components of vorticity and use equation $\omega_n = \vec{n} \cdot \vec{\omega}$ and the known ω_n to find the last boundary vorticity component. For example, if $|n_x| > |n_y|$ and $|n_x| > |n_z|$ then solve (17) for ω_y and ω_z and solve $\omega_n = \vec{n} \cdot \vec{\omega}$ for ω_x.

4.2. Heat flux

The heat flux is measured across all walls of the enclosure. It is reported in terms of the Nusselt number value. The wall average heat flux is measured by Nu, while the local heat flux is measured by the local Nusselt number value Nu_l. Since the heat flux is linearly interpolated across each boundary element, the local Nusselt number for i-th boundary element is defined by a surface integral over the element. So, the local and the average Nusselt numbers are defined as

$$Nu_{l,i} = \frac{1}{\Gamma_i} \int_{\Gamma_i} \frac{\partial T}{\partial n} d\Gamma, \quad Nu = \frac{1}{\Gamma} \sum_i \Gamma_i Nu_{l,i} = \frac{1}{\Gamma} \int_{\Gamma} \frac{\partial T}{\partial n} d\Gamma, \tag{18}$$

where Γ_i is the surface area of i-th boundary element of the wall and Γ is the surface area of the entire wall.

4.3. Computational mesh

In order to validate the numerical method and prove convergence of the results, we used several computational meshes. The meshes are composed of domain elements which enable quadratic interpolation of field functions and have 27 nodes. The mesh is set up in primary vortex $(x - z)$ plane and extruded into the third direction. The numerical algorithm is written in $3D$ and solves fully $3D$ flow problems. In order to simulate $2D$ phenomena, appropriate boundary conditions are used. Thus, two types of meshes are constructed: meshes for $2D$ simulations have only 1 element in y direction and meshes for $3D$ simulations have several elements in y direction.

Fig. 2 shows a quarter of the mesh. The other three-quarters of the mesh are symmetric. Letters A, B, C and D denote sides along which elements are distributed. The number of element along each side and the total number of nodes are listed in Table 2. The mesh elements are concentrated towards the walls in x and z directions. In y direction all elements have equal size.

4.4. Validation

In order to validate the numerical model, we performed simulations using air as the working fluid and compared results to Kim et al. [15], who studied natural convection of air in a square enclosure with a circular cylinder inserted in $2D$.
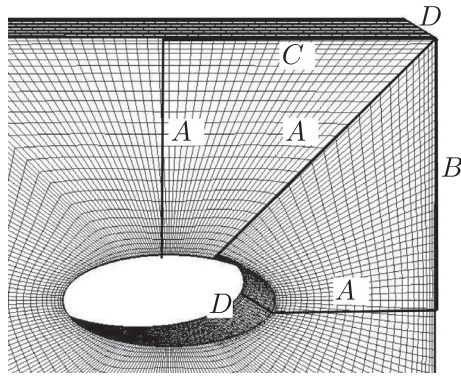
Fig. 2. Mesh design is based on specifying the number of elements along A, B, C and D sides. Hexahedra are used. Only a quarter of the mesh is shown, as the rest is symmetrical.

Table 2

Description of meshes used in this paper. The elements used are 27 node quadratic hexahedral Lagrange elements. The number of elements along sides and the total number of nodes is presented; see Fig. 2 for graphical representation of the sides.

Mesh name	Number of nodes ($\cdot 10^3$)	No. of elements along sides	
		Circle, $e = 0$ A, B, D, C	Ellipse, $e = 0.9$ A, B, D, C
$3D$ – fine	136	14, 14, 14, 10	14, 16, 12, 10
$3D$ – coarse	57.1	10, 10, 10, 8	12, 8, 12, 8
$2D$ – very fine	39.4	20, 20, 20, 1	20, 24, 16, 1
$2D$ – fine	32.0	18, 18, 18, 1	18, 22, 14, 1
$2D$ – coarse	14.4	12, 12, 12, 1	12, 14, 10, 1

Comparison is done for Rayleigh number values $Ra = 10^3 - 10^6$. The flow regime is laminar and steady. Heat transfer from the cylinder into the fluid is measured in terms of the Nusselt number. Three computational meshes are considered. Comparison is presented in Table 3. We observe good agreement with the results of Kim et al. [15], who studied the 2D case. Looking at the results on the fine mesh, we observe all Nusselt number values are within 1% of the Kim's results.

Simulations were repeated for the 3D case. No comparison is available in the literature, however we used two meshes to assess the required mesh density. Looking at the results on different meshes, we observe convergence of results. Based on this, we decided to use the 2D and 3D fine meshes for all simulations presented in the results section.

5. Results

We simulated pure water and six nanofluids, namely Al_2O_3, Cu, TiO_2 with nanoparticle volume fractions of $\varphi = 0.1$ and $\varphi = 0.2$. 2D simulations were done for four Rayleigh number values $Ra = 10^3 \ldots 10^6$, while in the 3D case, three Rayleigh number values were considered $Ra = 10^3 \ldots 10^5$. In terms of geometry we considered two 3D cases: a circular cylinder and an elliptical cylinder. For the 2D case we simulated five cases: a circular cylinder and elliptical cylinder under four inclinations $\gamma = 0° \ldots 45°$. In total we obtained results of 192 simulations. In the following section heat transfer expressed in terms of the Nusselt number plots is shown for all simulations. Other details such as contours, local Nusselt number plots and streamline plots are, due to the lack of space, shown only for selected cases. The complete simulation database is available upon request.

5.1. Circular cylinder

Since the cylinder is heated above the temperature of the surrounding fluid, the heat is transferred from the cylinder into the fluid. Hot fluid around the cylinder exhibits buoyancy forces and starts to raise against gravity. As it reaches the top wall, it turns towards the side walls creating two vortices one on each side of the enclosure. Streamlines for the case of $\varphi = 0.1$ copper nanofluids are shown in Fig. 3. At $Ra = 10^4$ the flow field is symmetrical and features four vortices in the top left, top right, bottom left and bottom right corners. As the temperature difference between the cylinder and the walls is small in this case, the flow field exhibits top to bottom symmetry as well as left–right symmetry. As the temperature difference is increased (middle and right panel of Fig. 3) we observe a break-up of top–bottom symmetry. Hot fluid close to the cylinder rises upwards and flows downwards along the vertical wall. The velocity magnitude is highest close to the cylinder.

Temperature contours for pure water and $\varphi = 0.1$ copper nanofluids are shown in Fig. 4. We observe little difference between water and nanofluid at the lowest Rayleigh number. In this case most of the heat is transferred via conduction and flow has a very small impact on temperature distribution. At higher Rayleigh number values, the differences are more visible, especially at the top of the cylinder. There, in the case of pure water, the contours are narrower than in the case of the nanofluid. This indicates that the area, where heat transfer is small (at the top of
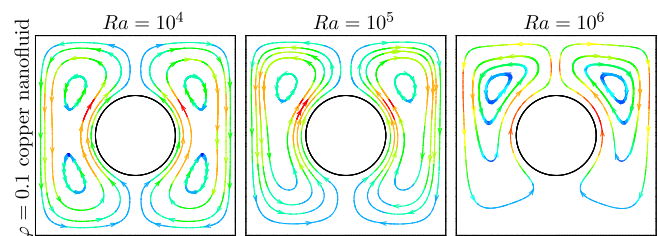

Fig. 3. Streamlines in a 2D simulation of $\varphi = 0.1$ copper nanofluid. Streamline colour denotes velocity magnitude.

Table 3

Validation of the numerical method. Average Nusselt number values at the hot cylinder for different values of the Rayleigh number are compared with the results of [15]. Simulations are performed in 2D and 3D on several meshes using air ($Pr = 0.7$) as the working fluid.

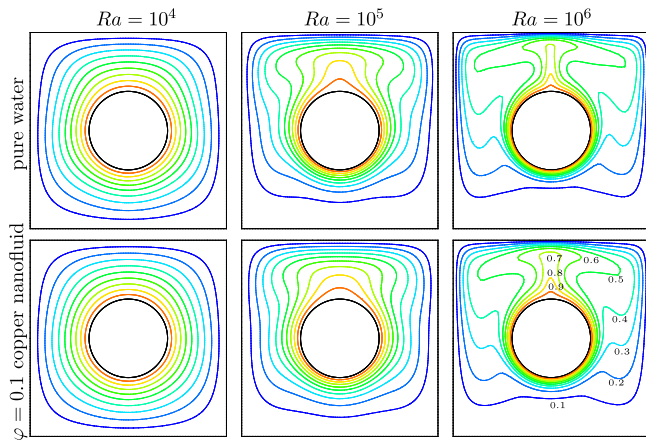| Mesh	Circle, $e = 0$				Ellipse, $e = 0.9$			
	10^3	10^4	10^5	10^6	10^3	10^4	10^5	10^6
$2D$ – very fine	5.041	5.133	7.756	14.020	5.079	5.288	8.760	14.595
$2D$ – fine	5.041	5.133	7.779	14.080	5.078	5.289	8.791	14.661
$2D$ – coarse	5.042	5.135	7.834	14.275	5.075	5.283	8.844	15.077
Kim et al. [15]	5.093	5.108	7.767	14.110				
$3D$ – fine	5.041	5.117	7.520		5.077	5.245	8.588	
$3D$ – coarse	5.040	5.115	7.514		5.075	5.243	8.599	

Fig. 4. Temperature contours in 2D simulation. Top panels show results of a pure water simulation, bottom panels present $\varphi = 0.1$ copper nanofluid. Nine contour levels are shown with values between 0.1 and 0.9 in steps of 0.1.

the cylinder) is smaller in the case of water than in the case of nanofluid.

Fig. 5 shows the average heat flux out of the circular cylinder into the fluid expressed as the Nusselt number value. We compare pure water and all three nanofluids and two nanoparticle concentrations. An increase of heat transfer with the Rayleigh number is evident in all cases. Since the Rayleigh number measures the temperature difference between the cylinder and surrounding walls, this increase is expected. The increase in the heat flux is minimal between $Ra = 10^3$ and $Ra = 10^4$. For these two cases, conduction is the dominant heat transfer mechanism (circular temperature contours in Fig. 4), thus increased buoyancy forces, which result in increased flow around the cylinder, are negligible and do not contribute to heat flux. As the temperature difference is increased further, the heat flux increases.

Taking a look at the differences between water and nanofluids we observe the following. Pure water has the lowest heat transfer rate, $\varphi = 0.1$ nanofluids show an increase, while $\varphi = 0.2$ nanofluids exhibit the largest heat transfer. The largest heat transfer enhancement is observed in the conduction dominated flow ($Ra = 10^3, 10^4$). In this flow regime the enhanced thermal properties of the nanofluid enable better heat transfer rate. As convection becomes important ($Ra \geq 10^5$) most of the heat is transferred by convection and thus the heat conductivity of the working fluid is not very important. Although we still observe an increase in heat transfer, it is relatively smaller than the increase in the conduction dominated flow regime.
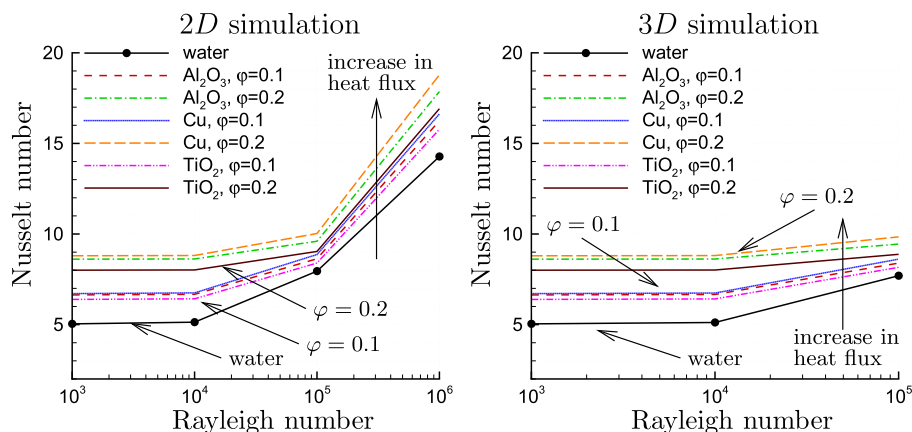
Comparing the results of the 2D and 3D simulations, we observe no major differences in heat transfer enhancement. The 3D simulation consistently shows slightly smaller heat transfer rates. This can be explained by looking at the 3D structure of the flow, which shows that the flow in the direction along a cylinder (y) is weak compared to the dominating vortex in the $x - z$ plane. Isosurfaces of y component of velocity, v_y for $\varphi = 0.1$ Al$_2$O$_3$ nanofluid are shown in Fig. 6. A break in symmetry is observed in the 3D structure of the flow field as Rayleigh number is increased. At low Rayleigh number the flow is symmetrical above and below the cylinder. This symmetry is lost when the Rayleigh number is increased. At $Ra = 10^5$ stronger motion in the direction along the cylinder is observed above the cylinder. As a smaller portion of heat is transferred from the top of the cylinder this 3D nature of the flow has a small impact on the overall heat transfer.

Fig. 7 shows the local heat flux around the circumference of the cylinder expressed at the local Nusselt number. Water and Al$_2$O$_3$ nanofluid are compared. At low Rayleigh number values ($Ra \leq 10^4$) we observe that the heat flux is approximately constant all around the cylinder. This is due to the fact that conduction is the driving heat transfer mechanism and thus heat enters the fluid equally in all directions. When convection becomes important ($Ra \geq 10^5$), upward flow around the cylinder is the main driving force of heat transfer. At the top of the cylinder, at around $\alpha = 90°$, there is an area where flow stagnates and we observe the lowest heat transfer there. On the other side, at the bottom of the cylinder, at around $\alpha = 270°$, the flow is fast and the temperature boundary layer is thin. Thus, we observe the highest heat transfer there. This situation is found in water and in nanofluids. In conduction regime the increase in heat transfer by nanofluids is mainly caused by the increased thermal properties of the nanofluid. In the convection regime, most of the heat is transferred by convection and thus the thermal properties of the fluid play a less important role and so we observe smaller heat transfer enhancement.

5.2. Elliptical cylinder

In the case of the elliptical cylinder, we considered several Rayleigh number values as well as different angles of inclination versus gravity. The elliptical shape causes a change in flow regime when tilted against gravity. To illustrate this point we choose TiO$_2$ nanofluid and present temperature contours and streamlines in Figs. 8 and 9. At $Ra = 10^4$ the heat transfer is conduction dominated and thus temperature contours keep the elliptical shape of the cylinder. Streamlines reveal a symmetrical flow field, with a
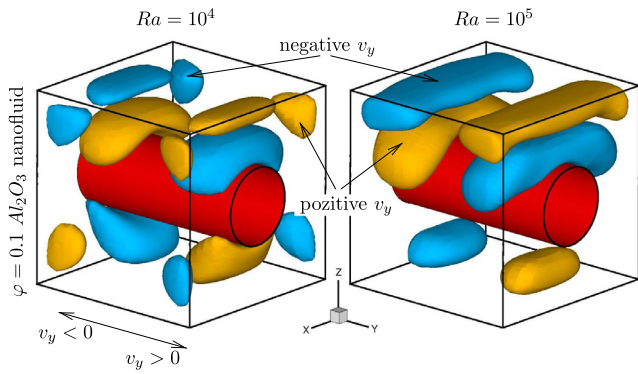

Fig. 5. Average heat flux out of the circular cylinder expressed as Nusselt number. Results of 2D simulations are shown in the left panel, 3D results are in the right panel.

Fig. 6. Isosurfaces of y component of velocity, v_y, for $\varphi = 0.1$ Al_2O_3 nanofluid. A major change is observed in the 3D structure of the flow field as Rayleigh number is increased.

vortex on both sides of the cylinder. Vortex centres are located approximately on a diagonal line going through the enclosure from the top-left corner to the bottom-right corner.

When we look at the convection dominated cases ($Ra = 10^5$ and $Ra = 10^6$) we observe that the symmetry is lost. Raising the tilt of the enclosure causes movement of the line, which divides both vortices. The location of this dividing line is important, as flow stagnates there and causes that area of the cylinder to have the lowest heat transfer. We observe that the line is located at the point of the cylinder, which is highest (has the largest z coordinate). Thus tilting the enclosure against gravity (raising γ) moves the low heat transfer zone away from the top of the cylinder ($\alpha = 90°$) towards the side ($\alpha = 0°$).

This can be also observed when we look at the heat flux distribution around the circumference of the cylinder in Fig. 10. On the other hand, in the conduction regime $Ra \leqslant 10^4$, the tilt against gravity does not affect the heat flux.

The heat flux distribution around the cylinder features two peaks at the sides of the enclosure. This is different than in the circular cylinder case, where the area with the highest heat transfer was located at the bottom of the cylinder (Fig. 7). Tilting the enclosure increases the heat transfer around most of the cylinder apart from the area around $\alpha = 0°$, where the heat flux is decreased. The highest heat transfer is found at bottom left side of the cylinder ($\alpha = 180°$).

The heat transfer averages expressed as Nusselt number values are given for zero tilt in Fig. 11 and for other tilts in Table 4. The data reveal heat transfer enhancement when using nanofluids instead of pure water. The enhancement is largest when conduction
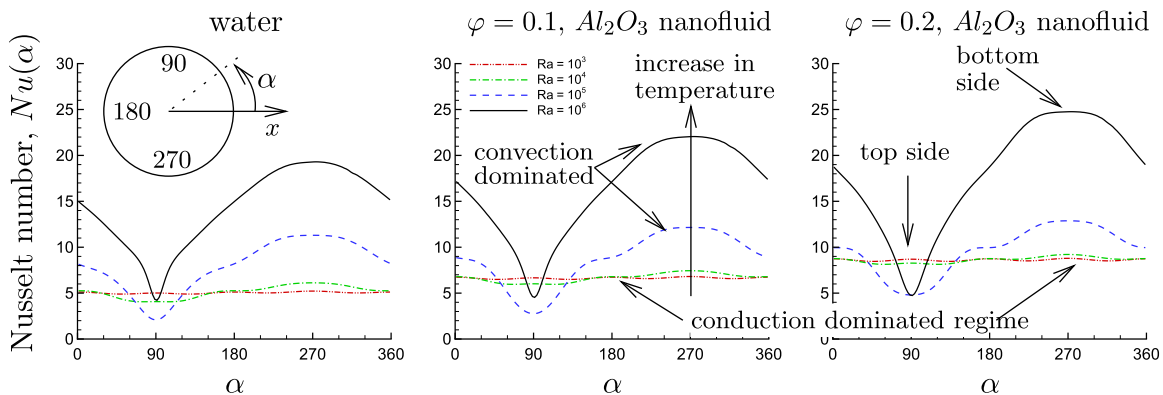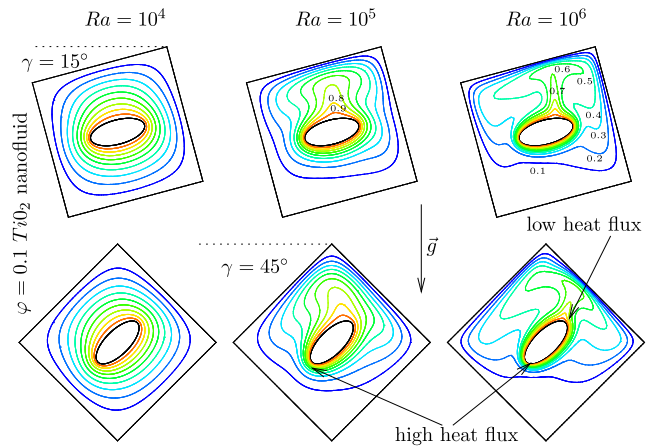

Fig. 8. Temperature contours of $\varphi = 0.1$ TiO_2 nanofluid in 2D simulation with elliptical cylinder for $Ra = 10^4 \ldots 10^6$. Top panels show results at $\gamma = 15°$, while bottom panels present $\gamma = 45°$. Nine contour levels are shown with values between 0.1 and 0.9 in steps of 0.1. (For interpretation of the references to color in this figure legend, the reader is referred to the web version of this article.)
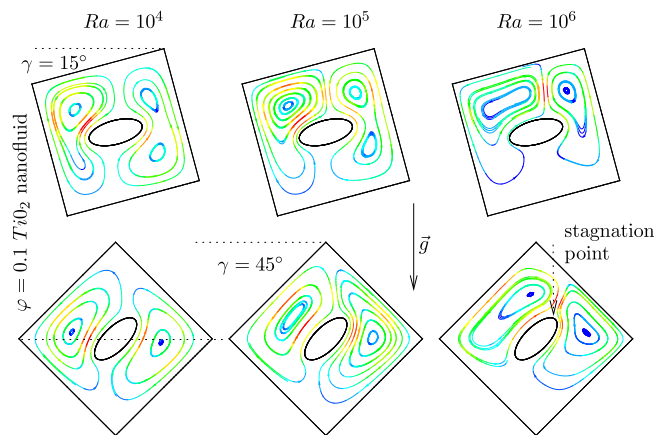

Fig. 9. Streamlines $\varphi = 0.1$ TiO_2 nanofluid in 2D simulation with elliptical cylinder for $Ra = 10^4 \ldots 10^6$. Top panels show results at $\gamma = 15°$, while bottom panels present $\gamma = 45°$. Colour denotes velocity magnitude.

is the dominating heat transfer mechanism ($Ra \leq 10^4$), where we observe about $\approx 30\%$ increase in heat flux for $\varphi = 0.1$ nanofluids and about $\approx 70\%$ increase when using $\varphi = 0.2$ nanofluids. As convection becomes important, enhancement is smaller, since fluid

Fig. 7. Heat flux around the circumference of the circular cylinder expressed as Nusselt number. Results of 2D simulations are shown. Pure water in the left panel, $\varphi = 0.1$ Al_2O_3 nanofluid in the centre panel and $\varphi = 0.2$ Al_2O_3 nanofluid in the right panel.
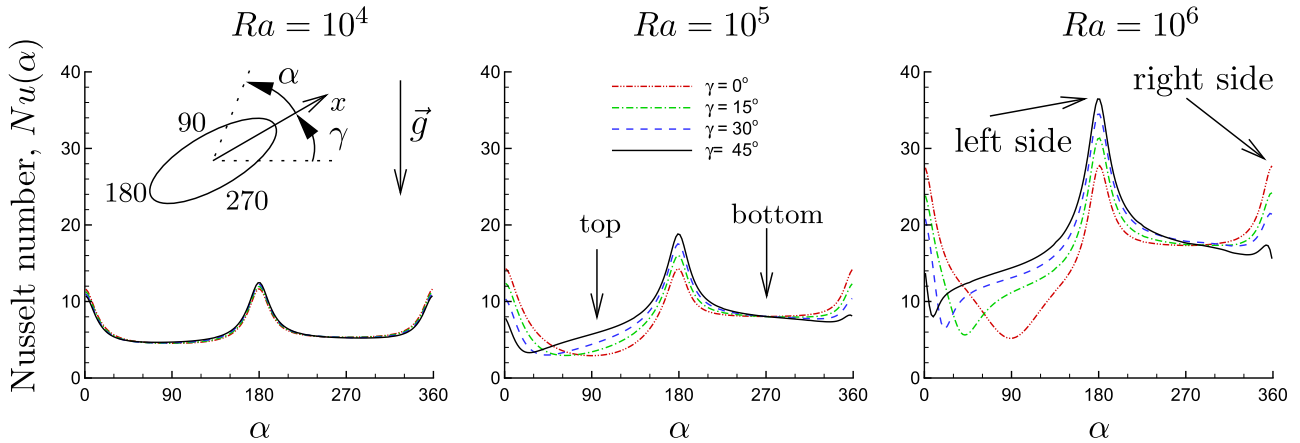
Fig. 10. Heat flux around the circumference of the ellipsoidal cylinder expressed as Nusselt number. Results of 2D simulations of $\varphi = 0.1$ Al$_2$O$_3$ nanofluid are shown for $Ra = 10^4$ (left), $Ra = 10^5$ (left) and $Ra = 10^6$ (right). Results for different angles γ against gravity are presented.

properties play a less important role in determining heat flux. For $Ra = 10^6$ we observe about $\approx 14\%$ increase in heat flux for $\varphi = 0.1$ nanofluids and about $\approx 30\%$ increase when using $\varphi = 0.2$ nanofluids.

Comparing the heat transfer averages for the circular and elliptic cylinders (Figs. 5 and 11) we observe that the results are similar, with the elliptical case exhibiting slightly larger heat transfer. In order to understand this, we consider a simplified problem of heat conduction through an insulation around a heated electrical wire. Let the wire and the outer surface of the insulation material be at constant temperatures. Heat is conducted through insulation. Since this case is geometrically simple (a cylinder within a cylinder) an analytical solution exists for temperature

$$T(r) = T_1 + \frac{T_2 - T_1}{\ln \frac{r_2}{r_1}} \ln \frac{r}{r_1}, \quad \frac{dT(r)}{dr} = \frac{T_2 - T_1}{r \ln \frac{r_2}{r_1}},$$

where r is the distance measured from the centre of the wire, r_1 is the radius of the wire and r_2 is the radius of the insulation. Calculating the temperature derivative at the wire gives $\frac{dT(r_1)}{dr} = \frac{T_2 - T_1}{r_1 \ln \frac{r_2}{r_1}}$ Using L as the characteristic length, the derivative may be written in nondimensional form as $Nu = \frac{L}{r_1 \ln \frac{r_2}{r_1}}$. Since in our circular case we have $r_1 = 0.2L$ and $r_2 \approx 0.5L$ we can calculate $Nu = 5.45$. For the elliptic case, we approximate the ellipse with an equal area circle, we get $r_1 = 0.15L$ and $Nu = 5.53$. Thus, this

Table 4
Average Nusselt number values for elliptical cylinder in 2D simulation.

γ/Ra	10^3	10^4	10^5	10^6	10^3	10^4	10^5	10^6
	$\varphi = 0.1$, Al$_2$O$_3$ nanofluid				$\varphi = 0.2$, Al$_2$O$_3$ nanofluid			
0	6.686	6.758	9.886	17.206	8.674	8.697	10.742	19.302
15	6.686	6.763	9.935	17.494	8.674	8.699	10.750	19.555
30	6.686	6.777	10.068	18.158	8.674	8.705	10.797	20.183
45	6.686	6.799	10.331	18.434	8.674	8.713	10.991	20.607
	$\varphi = 0.1$, Cu nanofluid				$\varphi = 0.2$, Cu nanofluid			
0	6.761	6.843	10.143	17.569	8.862	8.893	11.310	20.214
15	6.761	6.848	10.197	17.872	8.863	8.896	11.331	20.483
30	6.761	6.864	10.344	18.466	8.863	8.903	11.391	21.152
45	6.761	6.888	10.618	18.932	8.863	8.913	11.604	21.599
	$\varphi = 0.1$, TiO$_2$ nanofluid				$\varphi = 0.2$, TiO$_2$ nanofluid			
0	6.436	6.511	9.613	16.692	8.062	8.087	10.166	18.233
15	6.437	6.516	9.663	16.976	8.062	8.089	10.180	18.476
30	6.437	6.531	9.799	17.632	8.062	8.095	10.227	19.069
45	6.437	6.553	10.058	17.895	8.062	8.103	10.417	19.431
	Pure water, Pr = 6.2							
0	5.078	5.293	8.936	14.911				
15	5.079	5.300	9.017	15.248				
30	5.079	5.325	9.230	15.949				
45	5.080	5.371	9.486	16.396				

approximate analytical analysis yields a slight increase in Nu in the case of the elliptical cylinder, confirming our results.

Fig. 12 shows a comparison of heat flux expressed as the local Nusselt number value from the circular and elliptical cylinders.
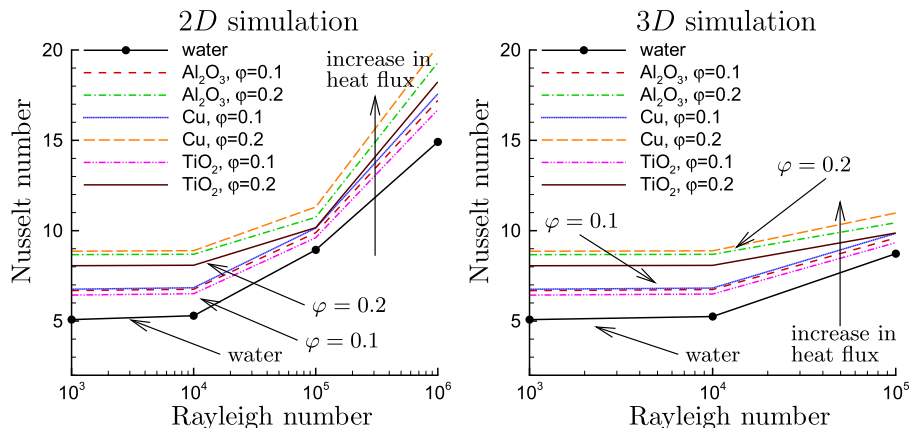

Fig. 11. Average heat flux out of the elliptical cylinder expressed as Nusselt number for $\gamma = 0$. Results of 2D simulations are shown in the left panel, 3D results are in the right panel.
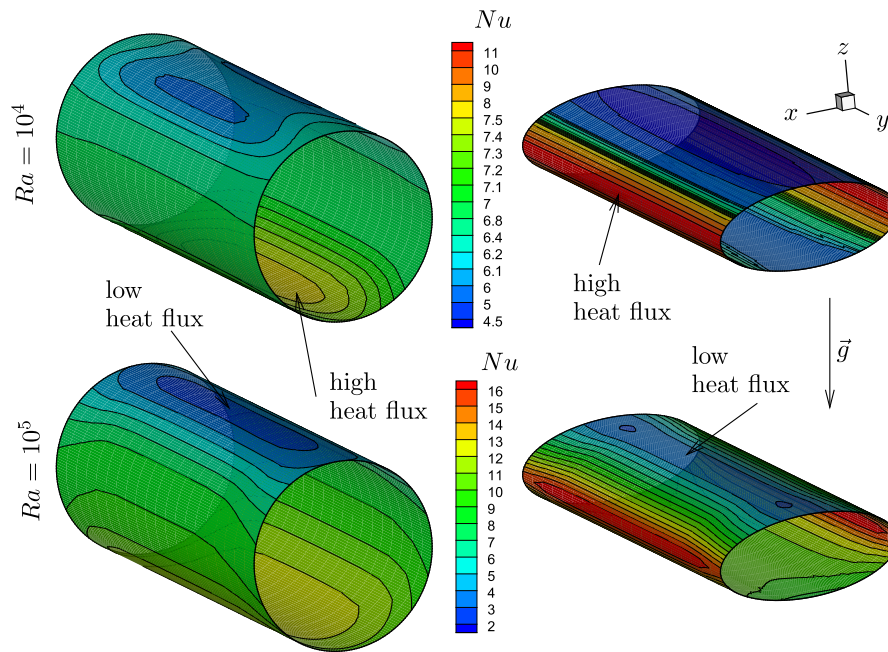
Fig. 12. Contours of heat flux around the circumference of cylinders expressed as Nusselt number for $\varphi = 0.1$ Cu nanofluid. Results of 3D simulations are shown for $Ra = 10^4$ (top), $Ra = 10^5$ (bottom).

We observe that in the circular cylinder case, the highest heat flux is located at the bottom of the cylinder, while in the elliptical case, the highest heat flux comes from the side of the cylinder. Considering the changes in heat flux along the y axis, we observe that in the central part of the cylinder the flow is predominantly two-dimensional, since changes in heat flux along the y axis are found only close to the enclosure walls.

6. Summary

The paper presents a boundary element based numerical method for simulation of flow and heat transfer of nanofluids. The Navier–Stokes equations are used in velocity–vorticity form. Special consideration was given to the algorithm for determining the boundary vorticity values at an arbitrary 3D boundary surface, which is based on the boundary-domain integral kinematics equation.

The developed method has been used to study nanofluid heat transfer enhancement for the case of a cylinder in an enclosure. Circular and elliptical cylinders were considered for various Rayleigh number values and inclinations against gravity.

The main conclusions of the analysis are: (1) Use of nanofluid enhances heat transfer the most in the case, where the majority of the heat is transferred by conduction. In cases, where convection is the dominant heat transfer mechanism, the heat transfer enhancement due to the use of a nanofluid is lower. (2) Comparing the circular and elliptic cylinders we observe similar heat transfer characteristics with the elliptical case yielding slightly better heat transfer rates. (3) Tilting the elliptical cylinder against gravity increases the heat transfer rate and changes the flow structure. The increase is small in flows, where conduction dominates, while it is larger in convection dominated flows. Furthermore it changes the locations on the cylinder, where lowest heat transfer is observed. (4) Comparison of 2D and 3D simulations shows, that 3D simulations yield slightly lower heat transfer rates. The difference is very small for conduction dominated flows, while in convection dominated flows it is larger. As the differences are small, 2D simulations may be used to analyse such problems.

Conflict of interest

None declared.

References

[1] M. El Abdallaoui, M. Hasnaoui, A. Amahmid, Numerical simulation of natural convection between a decentered triangular heating cylinder and a square outer cylinder filled with a pure fluid or a nanofluid using the lattice Boltzmann method, Powder Technol. 277 (2015) 193–205.
[2] E. Abu-Nada, H.F. Oztop, Effects of inclination angle on natural convection in enclosures filled with Cu–water nanofluid, Int. J. Heat Fluid Flow 30 (2009) 669–678.
[3] H.C. Brinkman, The viscosity of concentrated suspensions and solutions, J. Chem. Phys. 20 (1952) 571–581.
[4] S.U.S. Choi, Enhancing thermal conductivity of fluids with nanoparticles, Dev. Appl. Non Newtonian Flows 66 (1995) 99–106.
[5] O. Daube, Resolution of the 2D Navier–Stokes equations in velocity–vorticity form by means of an influence matrix technique, J. Comput. Phys. 103 (1992) 402–414.
[6] G.D.V. Davies, Natural convection of air in a square cavity: a bench mark numerical solution, Int. J. Numer. Methods Flow 3 (1983) 249–264.
[7] Hillal M. Elshehabey, F.M. Hady, Sameh E. Ahmed, R.A. Mohamed, Numerical investigation for natural convection of a nanofluid in an inclined l-shaped cavity in the presence of an inclined magnetic field, Int. Commun. Heat Mass Transfer 57 (2014) 228–238.
[8] Faroogh Garoosi, Gholamhossein Bagheri, Mohammad Mehdi Rashidi, Two phase simulation of natural convection and mixed convection of the nanofluid in a square cavity, Powder Technol. 275 (2015) 239–256.
[9] N.K. Ghaddar, F. Thiele, Natural convection over a rotating cylindrical heat source in a rectangular enclosure, Numer. Heat Transfer Part A 26 (1994) 701–717.
[10] C.J. Ho, M.W. Chen, Z.W. Li, Numerical simulation of natural convection of nanofluid in a square enclosure: effects due to uncertainties of viscosity and thermal conductivity, Int. J. Heat Mass Transfer 51 (2008) 4506–4516.
[11] Y. Hu, Y. He, C. Qi, B. Jiang, H.I. Schlaberg, Experimental and numerical study of natural convection in a square enclosure filled with nanofluid, Int. J. Heat Mass Transfer 78 (2014) 380–392.
[12] K.S. Hwang, J.-H. Lee, S.P. Jang, Buoyancy-driven heat transfer of water-based Al_2O_3 nanofluids in a rectangular cavity, Int. J. Heat Mass Transfer 50 (2007) 4003–4010.
[13] G.H.R. Kefayati, FDLBM simulation of entropy generation due to natural convection in an enclosure filled with non-Newtonian nanofluid, Powder Technol. 273 (2015) 176–190.
[14] K. Khanafer, K. Vafai, M. Lightstone, Buoyancy-driven heat transfer enhancement in a two-dimensional enclosure utilizing nanofluids, Int. J. Heat Mass Transfer 46 (2003) 3639–3653.

[15] B.S. Kim, D.S. Lee, M.Y. Ha, H.S. Yoon, A numerical study of natural convection in a square enclosure with a circular cylinder at different vertical locations, Int. J. Heat Mass Transfer 51 (2008) 1888–1906.

[16] C.H. Liu, Numerical solution of three-dimensional Navier Stokes equations by a velocity–vorticity method, Int. J. Numer. Methods Flow 35 (2001) 533–557.

[17] D.C. Lo, D.L. Young, K. Murugesan, C.C. Tsai, M.H. Gou, Velocity–vorticity formulation for $3D$ natural convection in an inclined cavity by DQ method, Int. J. Heat Mass Transfer 50 (2007) 479–491.

[18] M. Habibi Matin, I. Pop, Natural convection flow and heat transfer in an eccentric annulus filled by copper nanofluid, Int. J. Heat Mass Transfer 61 (2013) 353–364.

[19] J.C. Maxwell, A Treatise on Electricity and Magnetism, second ed., Clarendon Press, Oxford, UK, 1881.

[20] E.B. Ögüt, Natural convection of water-based nanofluids in an inclined enclosure with a heat source, Int. J. Therm. Sci. 48 (2009) 2063–2073.

[21] H.F. Oztop, E. Abu-Nada, Natural convection of water-based nanofluids in an inclined enclosure with a heat source, Int. J. Heat Fluid Flow 29 (2008) 1326–1336.

[22] M. Ramšak, Conjugate heat transfer of backward-facing step flow: a benchmark problem revisited, Int. J. Heat Mass Transfer 84 (2015) 791–799.

[23] J. Ravnik, L. Škerget, M. Hriberšek, Analysis of three-dimensional natural convection of nanofluids by BEM, Eng. Anal. Bound. Elem. 34 (2010) 1018–1030.

[24] J. Ravnik, L. Škerget, Z. Žunič, Velocity–vorticity formulation for $3D$ natural convection in an inclined enclosure by BEM, Int. J. Heat Mass Transfer 51 (2008) 4517–4527.

[25] J. Ravnik, L. Škerget, Z. Žunič, Combined single domain and subdomain BEM for $3D$ laminar viscous flow, Eng. Anal. Bound. Elem. 33 (2009) 420–424.

[26] S.M. Seyyedi, M. Dayyan, Soheil Soleimani, E. Ghasemi, Natural convection heat transfer under constant heat flux wall in a nanofluid filled annulus enclosure, Ain Shams Eng. J. 6 (1) (2015) 267–280.

[27] Mohsen Sheikholeslami, Mofid Gorji-Bandpy, Kuppalapalle Vajravelu, Lattice Boltzmann simulation of magnetohydrodynamic natural convection heat transfer of al2o3water nanofluid in a horizontal cylindrical enclosure with an inner triangular cylinder, Int. J. Heat Mass Transfer 80 (2015) 16–25.

[28] M.A. Sheremet, I. Pop, M.M. Rahman, Three-dimensional natural convection in a porous enclosure filled with a nanofluid using Buongiorno's mathematical model, Int. J. Heat Mass Transfer 82 (2015) 396–405.

[29] R.K. Shukla, V.K. Dhir, Numerical study of the effective thermal conductivity of nanofluids, in: ASME Summer Heat Transfer Conference, 2005.

[30] L. Škerget, M. Hriberšek, Z. Žunič, Natural convection flows in complex cavities by BEM, Int. J. Numer. Methods Heat Fluids Flow 13 (2003) 720–735.

[31] P. Ternik, Conduction and convection heat transfer characteristics of water–Au nanofluid in a cubic enclosure with differentially heated side walls, Int. J. Heat Mass Transfer 80 (2015) 368–375.

[32] X.-Q. Wang, A.S. Mujumdar, Heat transfer characteristics of nanofluids: a review, Int. J. Therm. Sci. 46 (2007) 1–19.

[33] K.L. Wong, A.J. Baker, A $3D$ incompressible Navier–Stokes velocity–vorticity weak form finite element algorithm, Int. J. Numer. Methods Fluids 38 (2002) 99–123.

[34] J.C. Wu, J.F. Thompson, Numerical solutions of time-dependent incompressible Navier–Stokes equations using an integro-differential formulation, Comput. Fluids 1 (1973) 197–215.

[35] Y. Yang, Z.G. Zhang, E.A. Grulke, W.B. Anderson, G. Wu, Heat transfer properties of nanoparticle-in-fluid dispersions (nanofluids) in laminar flow, Int. J. Heat Mass Transfer 48 (2005) 1107–1116.

[36] Z. Žunič, M. Hriberšek, L. Škerget, J. Ravnik, 3-D boundary element-finite element method for velocity–vorticity formulation of the Navier–Stokes equations, Eng. Anal. Bound. Elem. 31 (2007) 259–266.